


Specific capture of *Pseudomonas aeruginosa* for rapid detection of antimicrobial resistance in urinary tract infections

Journal Article**Author(s):**

[Pan, Fei](#) ; Altenried, Stefanie; Scheibler, Subas; Anthis, Alexandre H.C.; Ren, Qun

Publication date:

2023-02-15

Permanent link:

<https://doi.org/10.3929/ethz-b-000584903>

Rights / license:

[Creative Commons Attribution 4.0 International](#)

Originally published in:

Biosensors and Bioelectronics 222, <https://doi.org/10.1016/j.bios.2022.114962>



Specific capture of *Pseudomonas aeruginosa* for rapid detection of antimicrobial resistance in urinary tract infections

Fei Pan^{a,*}, Stefanie Altenried^a, Subas Scheibler^{b,c}, Alexandre H.C. Anthis^{b,c}, Qun Ren^{a,**}

^a Laboratory for Biointerfaces, Empa, Swiss Federal Laboratories for Materials Science and Technology, Lerchenfeldstrasse 5, 9014, St. Gallen, Switzerland

^b Nanoparticle Systems Engineering Laboratory, Institute of Process Engineering, Department of Mechanical and Process Engineering, ETH Zürich, Sonneggstrasse 3, 8092, Zürich, Switzerland

^c Laboratory for Particles Biology Interactions, Empa, Swiss Federal Laboratories for Materials Science and Technology, Lerchenfeldstrasse 5, 9014, St. Gallen, Switzerland

ARTICLE INFO

Keywords:

Urinary tract infections
Pseudomonas aeruginosa
Antimicrobial resistance
Magnetic nanoclusters
Specific capture
Rapid detection

ABSTRACT

Urinary tract infections (UTIs) are among the most predominant microbial diseases, leading to substantial healthcare burdens and threatening human well-being. UTIs can become more critical when caused by *Pseudomonas aeruginosa*, particularly by antimicrobial-resistant types. Thereby a rapid diagnosis and identification of the antimicrobial-resistant *P. aeruginosa* can support and guide an efficient medication and an effective treatment toward UTIs. Herein, we designed a platform for prompt purification, and effective identification of *P. aeruginosa* to combat the notorious *P. aeruginosa* associated UTIs. A peptide (QRKLAAKLT), specifically binding to *P. aeruginosa*, was grafted onto PEGylated magnetic nanoclusters and enabled a successful capture and enrichment of *P. aeruginosa* from artificial human urine. Rapid identification of antimicrobial resistance of the enriched *P. aeruginosa* can be moreover accomplished within 30 min. These functionalized magnetic nanoclusters demonstrate a prominent diagnostic potential to combat *P. aeruginosa* associated UTIs, which can be extended to other *P. aeruginosa* involved infections.

1. Introduction

Urinary tract infections (UTIs) are among the most prevalent microbial diseases and consume substantial public finance (Leitner et al., 2021). Complicated UTIs are among the major causes of bacteremia and are related to a high mortality rate for critically ill patients (Chan and Yuen, 2015; To et al., 2013; Wagenlehner et al., 2008). Additionally, recurrent UTIs are common among young and healthy females, although they generally possess normal urinary tracts in the anatomical and physiological regards (Finer and Landau, 2004). Toward UTIs, particularly complicated UTIs, broad-spectrum antibiotics are empirically employed against uropathogenic Gram-negative bacteria (Chan and Yuen, 2015; Flores-Mireles et al., 2015). However, UTIs have led to the majority of antibiotic prescriptions in European nursing homes, but most of such antibiotic prescriptions are improper (Arnold et al., 2021; Ricchizzi et al., 2018). Overuse and misuse of antibiotics are the major cause of antimicrobial resistance (AMR) (Roberts and Zembower, 2021;

Pan, 2022). Most UTIs are associated with *Escherichia coli*, and the related threats to human well-being are intensively studied (Roberts and Zembower, 2021; Hoban et al., 2011). However, UTIs caused by *P. aeruginosa* are lacking in studies, even though *P. aeruginosa* UTIs are associated with high mortality in hospitalized patients and can lead to even more complicated treatments, likely due to the *P. aeruginosa* intrinsic resistance to multiple antibiotics (Lamas Ferreiro et al., 2017). Thereby, it is imperative to obtain the AMR profile of *P. aeruginosa* from UTIs before the antibiotic prescription.

Despite the substantial advances made, the AMR diagnostics still faces huge challenges. One of the challenges is the long turnaround time, particularly for samples with a low number of targeted pathogens. Pre-culture steps are required to enrich the microbes present and purify them. Antibodies have also been used to recover bacteria due to their high specificity toward target antigens on the surfaces of pathogens (Lesniewski et al., 2014). However, the antibody preparation is complex and costly, and very few antibodies for specific targets are available (Lai

* Corresponding author.

** Corresponding author.

E-mail addresses: Fei.Pan@empa.ch, Fei.Pan@unibas.ch (F. Pan), Qun.Ren@empa.ch (Q. Ren).

¹ Present address: Department of Chemistry, University of Basel, Mattenstrasse 24a, BPR 1096, 4058 Basel, Switzerland. Fei.Pan@unibas.ch

et al., 2015). Furthermore, antibodies are usually very large and difficult to immobilize on a given surface, especially a sphere surface, limiting their widespread applications in particle-based pathogenic bacteria detection (Lai et al., 2015). Apart from antibodies, some antibiotics, proteins (such as avidin, biotin, lectin et al.), DNA/RNA aptamers, and carbohydrates (such as glycan) have also been used as targeting ligands to probe target bacteria (Bohara and Pawar, 2015). However, poor specificity is one of the general problems with these approaches. Herein, we propose a diagnostic system to address the abovementioned challenges by utilizing a specific peptide to precisely capture *P. aeruginosa* without pre-culture of the samples to be analyzed.

Magnetic nanoparticles (MNPs) have been applied to isolate bacterial pathogens through magnetic capture (Lattuada et al., 2016). To ensure the stability of the MNPs (Jokerst et al., 2011), MNPs coated with polyethylene glycol (PEG) were purchased and used in this work. For specific capture of *P. aeruginosa*, the peptide QRKLAAKLT, discovered via phage-display screening, was used due to its capability of specific and strong binding to the outer membrane of *P. aeruginosa* (Carnazza et al., 2008). QRKLAAKLT was utilized to functionalize magnetic nanoclusters (MNCs) for specific isolation and enrichment of *P. aeruginosa* pathogens, followed by rapid determination of AMR pathogens through applying a luminescence-based method (Scheme 1).

2. Materials and methods

2.1. Materials

Chemicals and reagents of analytical purity were all purchased from Sigma-Aldrich (Buchs, Switzerland) and employed as received unless otherwise noted. Dextran iron oxide composite nanoclusters (MNCs, Product code: 09-00-132, 25 g L⁻¹, 130 nm) and PEG-NH₂ functionalized dextran iron oxide composite nanoclusters (PEGylated MNCs,

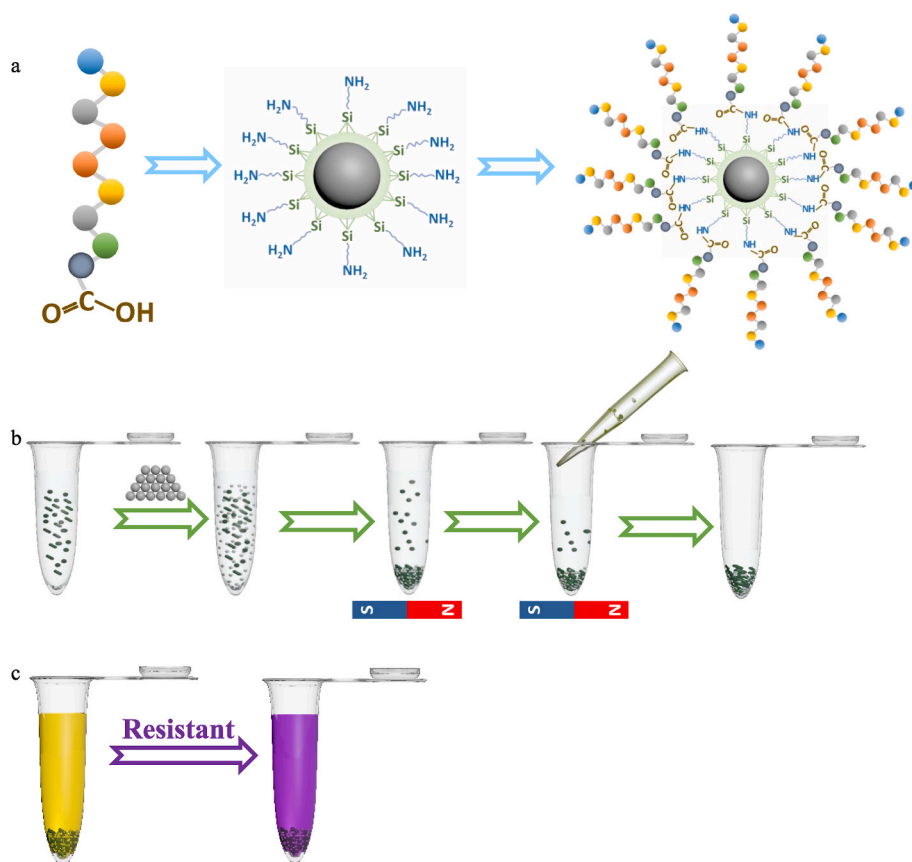
Product code: 09-55-132, 10 g L⁻¹, 130 nm) were ordered in aqueous suspension from micromod Partikeltechnologie GmbH (Rostock, Germany). Phosphate-buffered saline (PBS) at pH 7.4 was prepared as follows: 8 g L⁻¹ NaCl, 0.2 g L⁻¹ KH₂PO₄, and 1.44 g L⁻¹ Na₂PO₄ with distilled water. Bacterial growth medium (LB broth) was prepared as follows: 10 g L⁻¹ tryptone, 5 g L⁻¹ yeast extract, and 5 g L⁻¹ NaCl with distilled water. Broth media of an adjusted pH 7.4 was prepared: 5 g L⁻¹ peptone, 5 g L⁻¹ NaCl, 2 g L⁻¹ yeast extract, 1 g L⁻¹ beef extract. Artificial urine was prepared (Sarigul et al., 2019) with following ingredients: 1.7 g L⁻¹ Na₂SO₄, 0.25 g L⁻¹ C₅H₄N₄O₃, 0.72 g L⁻¹ Na₃C₆H₅O₇·2H₂O, 0.881 g L⁻¹ C₄H₇N₃O, 15 g L⁻¹ CH₄N₂O, 2.308 g L⁻¹ KCl, 1.756 g L⁻¹ NaCl, 0.185 g L⁻¹ CaCl₂, 1.266 g L⁻¹ NH₄Cl, 0.035 g L⁻¹ K₂C₂O₄·H₂O, 1.082 g L⁻¹ MgSO₄·7H₂O, 2.912 g L⁻¹ NaH₂PO₄·2H₂O, 0.831 g L⁻¹ Na₂HPO₄·2H₂O in distilled water.

2.2. Functionalization kinetics of magnetic nanoclusters

A peptide (QRKLAAKLT, final concentration of 0.02 mM, 0.2 mM, 1 mM, 2 mM, and 20 mM) specific to *P. aeruginosa*, screened from bacteriophage display library (Franco et al., 2020), was added to MNCs and PEGylated MNCs of a final concentration 9 g L⁻¹ for both MNCs. Both mixtures were shaken for 2 h at 100 rpm and 25 °C. The MNCs in every suspension were subsequently collected and rinsed through three centrifugations at 14400 rpm and 25 °C. After every centrifugation, the supernatant was then replaced by the same amount of fresh PBS.

2.3. XPS analysis

An X-ray photoelectron spectroscopy (XPS, PHI 5000 VersaProbe II instrument with a monochromatic AlK α X-ray source, USA) was utilized to assess the surface chemical properties of the samples (Wei et al., 2022a, 2022b; Lai et al., 2019; Tong et al., 2013).



Scheme 1. Scheme of the rapid detection of antimicrobial resistance. (a) QRKLAAKLT was utilized to functionalize PEGylated magnetic nanoclusters (PEG@MNCs); (b) The peptide-modified PEG@MNCs (peptide@PEG@MNCs) were applied to interact with bacterial suspensions and subsequently enabled a bacterial collection under a magnetic field; (c) A sensitive luminescence-based method was employed to assess the growth of the collected bacterial pathogens in the presence of antibiotics in order to distinguish susceptible and resistant bacteria.

2.4. Vibrating sample magnetometry

The vacuum-dried sample was added to the polymer-sample holders and analyzed by vibrating sample magnetometry (VSM) utilizing the physical properties measurement system (PPMS, Version P525, Quantum Design GmbH Germany) of Quantum Design at a maximum magnetic field of 5T.

2.5. Dynamic light scattering (DLS)

The hydrodynamic size of different samples was analyzed through a DLS instrument (ZetaSizer90, Malvern) at a refractive index of iron oxide ($n = 2.918$). MNCs suspensions were diluted to a final concentration of 0.9 g L^{-1} and were briefly sonicated for 30 s before measurement.

2.6. TEM analysis

TEM analysis was executed through the utilization of a JEOL TEM equipped with an in-column Omega-type energy filter (JEM-2200FS, Joel, Japan) (Wu et al., 2021, 2022a, 2022b; Pan et al., 2016, 2017, 2022a; Guo et al., 2022). 5 μL of the sample after a 100-fold dilution was added to a TEM grid (Kung et al., 2018, 2020; Tseng et al., 2020) (Carbon Film Supported Copper Grid, 200 Meshes, Electron Microscopy Sciences, USA) till the solvent was completely evaporated (Yang et al., 2022; Pan et al., 2022b; Yu et al., 2021; Kung et al., 2021).

2.7. Cytotoxicity analysis

The cytotoxic analysis toward the PEG@MNCs and peptide@PEG@MNCs was performed with normal human dermal fibroblasts (nHDFs, female, caucasian, skin/temple, PromoCell, C-12352). Every sample (final concentration: 9 g L^{-1} as no dilution) was centrifugated, and the supernatant was replaced with DMEM (Dulbecco's Modified Eagle Medium) containing 1% penicillin/streptomycin/neomycin (PSN). Every sample was parallelly analyzed by negative control (empty wells) and its additional dilutions (2X, 4X, 8X, 16X, 32X, 64X, and 128X). 10 000 nHDFs in 100 μL DMEM containing 10% foetal calf serum (FCS) were seeded into every well (TPP, Trasadingen, Switzerland) for 24 h before incubating with the sample solutions. Subsequently, the nHDFs were incubated for 24 h with 100 μL solutions containing 95% sample solution and 5% FCS. The viability of nHDFs from the negative control was set as 100%, and the one that interacted with 1% Triton X-100 in DMEM containing 5% FCS was considered as the positive control. The viability of the nHDFs was analyzed through MTS [(3-(4,5-Dimethylthiazol-2-yl)-5-(3-carboxymethoxyphenyl)-2-(4-sulfophenyl)-2H-tetrazolium)] assay at the absorbance 490 nm to measure metabolic activity of the nHDFs (Jin et al., 2013; Solar et al., 2015; Pan et al., 2022c; Huang et al., 2022).

2.8. Bacterial preparation

Escherichia coli DSMZ 30083, *Pseudomonas aeruginosa* DSMZ 1117, *Pseudomonas aeruginosa* ATCC 15442, *Staphylococcus aureus* ATCC 6538, *Staphylococcus epidermidis* ATCC 49461 were utilized in the bacterial capture assays. One bacterial colony of every bacterial strain from an agar plate was taken and incubated in 10 mL LB in a 50 mL Falcon tube at 160 rpm and 37 °C overnight. 100 μL overnight culture was added into 10 mL fresh LB and subsequently cultivated for approximately 2 h to reach exponential growth (Guo et al., 2022; Hegemann et al., 2022; Milionis et al., 2020).

2.9. Antimicrobial resistance (AMR) detection

P. aeruginosa DSMZ 1117 and *P. aeruginosa* ATCC 15442 were incubated in 10 mL LB containing $10 \mu\text{g mL}^{-1}$ Gentamicin in a 50 mL Falcon

tube at 160 rpm and 37 °C overnight to determine bacterial sensitivity and resistance to Gentamicin. The overnight bacterial culture of *P. aeruginosa* DSMZ 1117 and *P. aeruginosa* ATCC 15442 in LB containing $10 \mu\text{g mL}^{-1}$ Gentamicin displayed a clear and turbulent bacterial suspension, respectively. Consequently, as revealed, *P. aeruginosa* DSMZ 1117 and *P. aeruginosa* ATCC 15442 are respectively susceptible and resistant to Gentamicin. Therefore, *P. aeruginosa* DSMZ 1117 is referred to as susceptible *P. aeruginosa*, and *P. aeruginosa* ATCC 15442 is analogously referred to as resistant *P. aeruginosa*. The collected bacteria, through magnetic separation, were resuspended in Broth media. AquaSpark® caprylate (Product Code: A-8167_P00, Biosynth AG, Staad, Switzerland) was in the meanwhile diluted to a concentration of 0.5 mM with Trisma Buffer pH 7.0. 0.198 mL bacterial suspension was subsequently incubated with 2 μL diluted AquaSpark® solution for 20 min. Luminescence and optical density (OD_{600}) were continuously recorded for 6 h with a time interval of 0.5 h through a plate reader (PowerWave HT, BioTek instruments Inc., U.S.A.) (Lai et al., 2018).

2.10. Bacterial specific capture

The bacterial cultures of *E. coli*, susceptible and resistant *P. aeruginosa*, *S. aureus*, and *S. epidermidis* were diluted with sterile PBS as reported (Pan et al., 2020, 2021a, 2021b) to around 10^6 colony forming units (CFU) mL^{-1} . Then, 500 μL bacterial suspension was mixed (shaking at 160 rpm) respectively with 50 μL peptide modified PEG@MNCs, 50 μL peptide interacted MNCs, 50 μL PEG@MNCs and 50 μL MNCs for 10 min at 37 °C. Subsequently, these suspensions were placed under a magnetic field for 5 min, and the clear supernatants were then replaced with fresh 550 μL PBS. This rinsing process was processed 4 times more. The obtained samples were further diluted with fresh PBS, and thereafter 100 μL liquid sample was plated on PC-agar plates with three replicates. Observing bacterial colonies on PC-agar plates was performed after incubating the PC-agar plates for 12 h at 37 °C. This specific capture was additionally performed based on different times of the rinsing process: from no rinsing to 5 times rinsing.

2.11. Adhesion force analysis between bacteria and nanoclusters

MNCs (non-functionalized/functionalized on MNCs/PEG@MNCs) were immobilized on glass-bottom microscopy dishes (GWSB-5040, WillCo-Dish, Amsterdam, Netherlands) for force spectroscopy analysis, 2 mL 9 g L^{-1} MNCs were added and precipitated on polydopamine-coated glass-bottom microscopy dishes. Such glass-bottom microscopy dishes were coated with polydopamine with a reported method (Mittelviehhaus et al., 2019; Pan et al., 2022d). Briefly, the bottom glass of the microscopy dishes was washed with 2-propanol with sonication and afterward deionized water. Then N_2 -stream was applied to dry the washed bottom glass of these microscopy dishes before treatment with air plasma for 120 s (Plasma Cleaner PD-32G, Harrick Plasma, USA). 4 mL 4 g L^{-1} polydopamine (in 10 mM TRIS HCl, pH 8.5) was used to immerse the bottom glass for 60 min before thoroughly rinsing with PBS buffer. The MNCs were pipetted to the coated glass surfaces for 1 h. Thorough rinsing with PBS buffer subsequently removed the non-adhered MNCs on the glass surfaces. The immobilized MNCs were kept in 4 mL PBS to ensure a good immersion of the FluidFM cantilever in PBS buffer.

The Flex Bio-AFM (Nanosurf, Switzerland) and the digital pressure controller (Cytosurge, Switzerland) were similarly employed for the force spectroscopy measurements, as reported (Pan et al., 2022e). Single-bacterium force spectroscopy was similarly performed at room temperature in PBS buffer (pH 7.4) with *E. coli*, susceptible and resistant *P. aeruginosa*, *S. aureus*, and *S. epidermidis* as reported (Pan et al., 2022e).

2.12. Bacterial specific capture rate

The specific capture rate was performed similarly to the assay of

bacterial specific capture. However, the incubation time of bacterial suspension and every MNCs was defined as 5 min, 10 min, 30 min, 60 min, 90 min, and 120 min.

2.13. The sensitivity of the bacterial specific capture

The sensitivity of the specific capture was executed similarly to the assay of bacterial specific capture. However, the initial bacterial suspensions before incubation with the modified PEG@MNCs were additionally diluted as 10, 100, 1 000, 10 000, 100 000, and 1000 000 folds.

2.14. Bacterial specific capture in artificial urine

Bacterial specific capture in artificial urine was similarly carried out as in the assay of bacterial specific capture. Bacterial suspension mixtures were also prepared as follows with every bacteria of 10^6 CFU mL⁻¹: susceptible *P. aeruginosa* & *E. coli*, susceptible *P. aeruginosa* & *S. aureus*, susceptible *P. aeruginosa* & *S. epidermidis*, resistant *P. aeruginosa* & *E. coli*, resistant *P. aeruginosa* & *S. aureus*, resistant *P. aeruginosa* & *S. epidermidis*, and susceptible *P. aeruginosa* & resistant *P. aeruginosa*. Moreover, the resistance of the captured bacteria was analyzed with the aforementioned method.

2.15. Polymerase chain reaction (PCR) analysis

Primers (FtoxA-PA primer: 5'-TTCGTCAGGGCGCAGGAGAGCA-3' and RtoxA-PA primer: 5'-TCTCCAGCGGCAGGTGGCAAG-3'; 16SSAIII-SA:5'-TATAGATGGATCCGCGCT-3' and 16SSAIV-SA: 5'-GATTAGG-TACCGTCAAGAT-3'; forward primer targeting *E. coli*: 5'-CTGCTCTTTTAAGCAACTGGCGA-3' and reverse primer targeting *E. coli*: 5'-ACCAGACCCAGCACCAGATAAG-3') were employed to

amplify the region from the 5' of the upstream to the 3' of the downstream region of *tox A* gene of *P. aeruginosa*. PCR analyses were performed by using 200 μ L captured bacteria as DNA source, 200 μ M nucleotides (N0447S, NEB, USA), adequate primers (0.5 μ M), 3% DMSO, 1X Buffer Phusion HF, and 1 Unit mL⁻¹ Phusion DNA Polymerase (Phusion High-Fidelity DNA Polymerase, M0530, NEB, USA). Cycling conditions applied in this study were 98 °C for 360 s, followed by 31 cycles of 98 °C for 10 s, 58 °C for 30 s, and 72 °C for 90 s, and a final extension at 72 °C for 300 s. PCR products were subsequently analyzed by electrophoresis at 100 V for 60 min with 1% (w/v) agarosegel (V3125, Promega, Spain). The size obtained after every amplicon was compared to the 1 kb DNA ladder (GeneRuler 1 kb DNA Ladder, SM0333, Thermo Scientific, USA).

3. Results and discussion

3.1. Bacterial capture and rapid AMR detection

QRKLAAKLT peptide was first grafted to the PEGylated magnetic nanoclusters (PEG@MNCs) through covalent bonding between -COOH (peptide) and -NH₂ (PEG@MNCs). Five different concentrations of QRKLAAKLT peptide were employed to identify the most efficient grafting. Based on the X-ray photoelectron spectroscopy (XPS) analysis, the [C]/[O] elemental ratios were $78.3 \pm 0.4\%$, $203.5 \pm 2.1\%$, $209.2 \pm 4.2\%$, $359.2 \pm 13.9\%$, and $315.1 \pm 13.6\%$, respectively, for the peptide solutions of 0.02, 0.2, 1, 2 and 20 mM (Fig. 1a). The functionalization of the PEG@MNCs by employing the peptide solution of 2 mM yielded the highest [C]/[O] elemental ratio, revealing that grafting by this solution can confer the most efficient modification of the PEG@MNCs (peptide@PEG@MNCs, Fig. 1b), thus utilized for the subsequent analysis.

Based on the DLS analysis, the peptide@PEG@MNCs exhibited a size

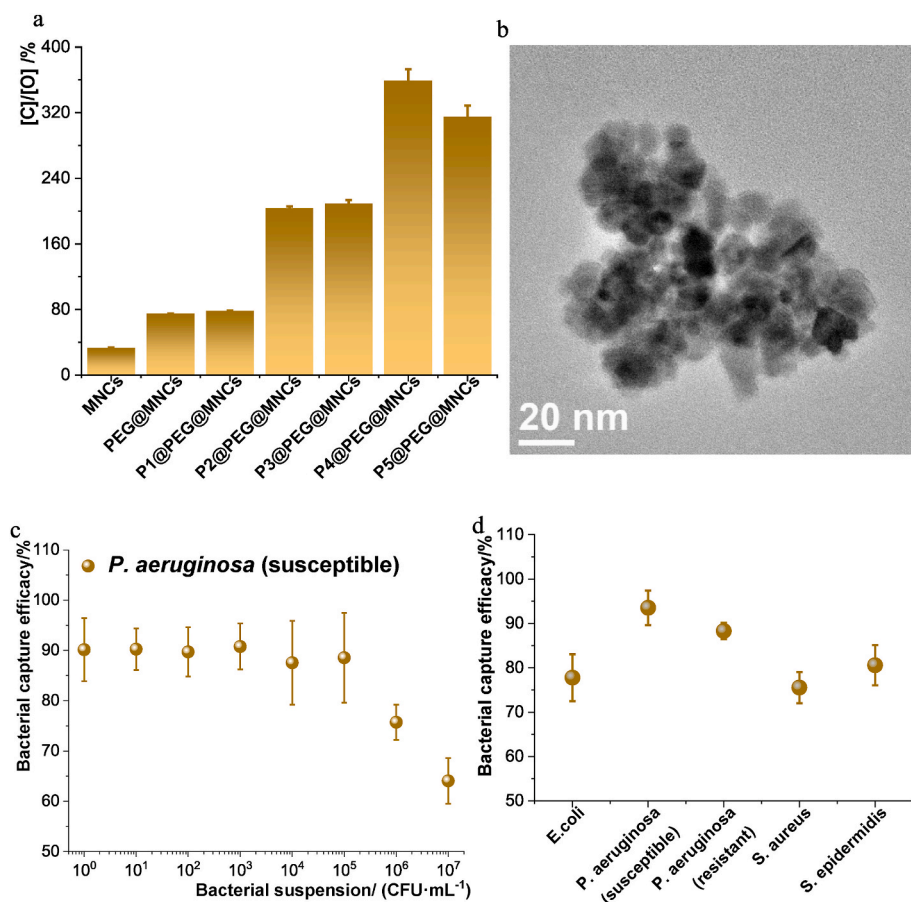


Fig. 1. Characterization of the modified MNCs and their capture ability toward bacterial pathogens without a rinsing process. (a) The elemental ratios of [C]/[O] were determined by utilizing XPS to analyze the functionalization efficiency of PEGylated MNCs by the peptide solutions of various concentrations. P1–P5 represented respectively peptide solutions of 0.02, 0.2, 1, 2, and 20 mM. (b) PEGylated MNCs modified by the peptide solution of 2 mM (peptide@PEG@MNCs) were imaged by a scanning transmission electron microscope (STEM), manifesting the peptide@PEG@MNCs of a cluster structure. (c) Capture capability analysis of the modified MNCs was performed toward susceptible *P. aeruginosa* of different concentrations and normalized to the initial bacterial concentration at every range. An initial bacterial suspension of 51700000 ± 2400000 CFU mL⁻¹ was considered for the concentration range of 10^7 CFU mL⁻¹, and the rest from 10^6 – 10^0 CFU mL⁻¹ was a stepwise reduction of one order of magnitude of 10^7 CFU mL⁻¹. (d) Bacterial capture efficiencies of the modified MNCs without a rinsing procedure toward *E. coli*, susceptible and resistant *P. aeruginosa*, *S. aureus*, and *S. epidermidis*, respectively, were normalized to the initial suspension of 339000 ± 23000 , 674000 ± 24000 , 145000 ± 17000 , 783000 ± 16000 and 684000 ± 20000 CFU mL⁻¹. n = 3 (biological repeats), mean \pm SD shown; at least two sets of independent experiments were performed, and one set of data is shown here.

of 146.6 ± 1.2 nm in diameter (Fig. S1a), slightly higher than the pristine PEG@MNCs of 142.9 ± 0.9 nm in diameter (Fig. S1a&b). Additionally, the peptide@PEG@MNCs and PEG@MNCs both manifested magnetic properties and no cytotoxicity (Fig. S1c&d, Fig. 1b). To evaluate the detection limit of the peptide@PEG@MNCs, we employed susceptible *P. aeruginosa* as a model strain of various concentrations (10^0 – 10^7 CFU mL⁻¹) in PBS buffer. The peptide@PEG@MNCs manifested its excellent capture capacity even in an extremely low concentration range of 10^0 CFU mL⁻¹. However, the capture efficiency decreased once the bacterial concentration reached 10^6 CFU mL⁻¹ (Fig. 1c). Hence, we applied bacterial concentrations below 10^6 CFU mL⁻¹ for further analysis. To insight the specificity of the bacterial capture by the developed peptide@PEG@MNCs, different bacterial pathogens with a concentration of about 10^5 CFU mL⁻¹ were tested, including *E. coli*, susceptible and resistant *P. aeruginosa*, *S. aureus*, and *S. epidermidis* (Fig. 1d). Bacterial capture efficiency of over 75% was obtained for all the examined bacterial strains within 10 min (Fig. 1d), manifesting that the peptide@PEG@MNCs could efficiently remove bacterial pathogens from the infected systems. Since the non-specific interaction between bacteria and peptide@PEG@MNCs could lead to a high bacterial capture efficiency, we thereby introduced a rinsing process to test the specificity. Susceptible *P. aeruginosa* and *S. aureus* were utilized as examples, followed by a five-time rinsing procedure. The

rinsing process has rarely been done to the best of our knowledge, leading to the high bacterial capture specificity; thus, it is difficult to define the specificity of the previous work toward bacterial capture (Lattuada et al., 2016). However, the capture efficiency for both strains was compromised with every rinsing step. After five-time rinsing, only susceptible *P. aeruginosa* was detected, with a capture efficiency of over 40% (Fig. 2a). Therefore, the rinsing process removed the weakly, non-specific bound bacteria from the peptide@PEG@MNCs, and the strongly bound *P. aeruginosa* was retained, yielding a specific capture. Hence, the designed peptide@PEG@MNCs can specifically capture *P. aeruginosa* after applying the rinsing process, and, additionally, are capable of isolating various bacteria without the rinsing steps (Fig. 1d and 2a).

3.2. Specific capture of *P. aeruginosa*

The specific binding of the peptide@PEG@MNCs was further analyzed with a five-time rinsing procedure toward *E. coli*, susceptible and resistant *P. aeruginosa*, *S. aureus*, and *S. epidermidis* using the MNCs, PEG@MNCs, and peptide@MNCs as controls (Fig. 2). With the rinsing process, only the susceptible and resistant *P. aeruginosa* were captured after incubation with the peptide@PEG@MNCs, whereas the other strains and nanoclusters did not lead to sufficient bacterial capture

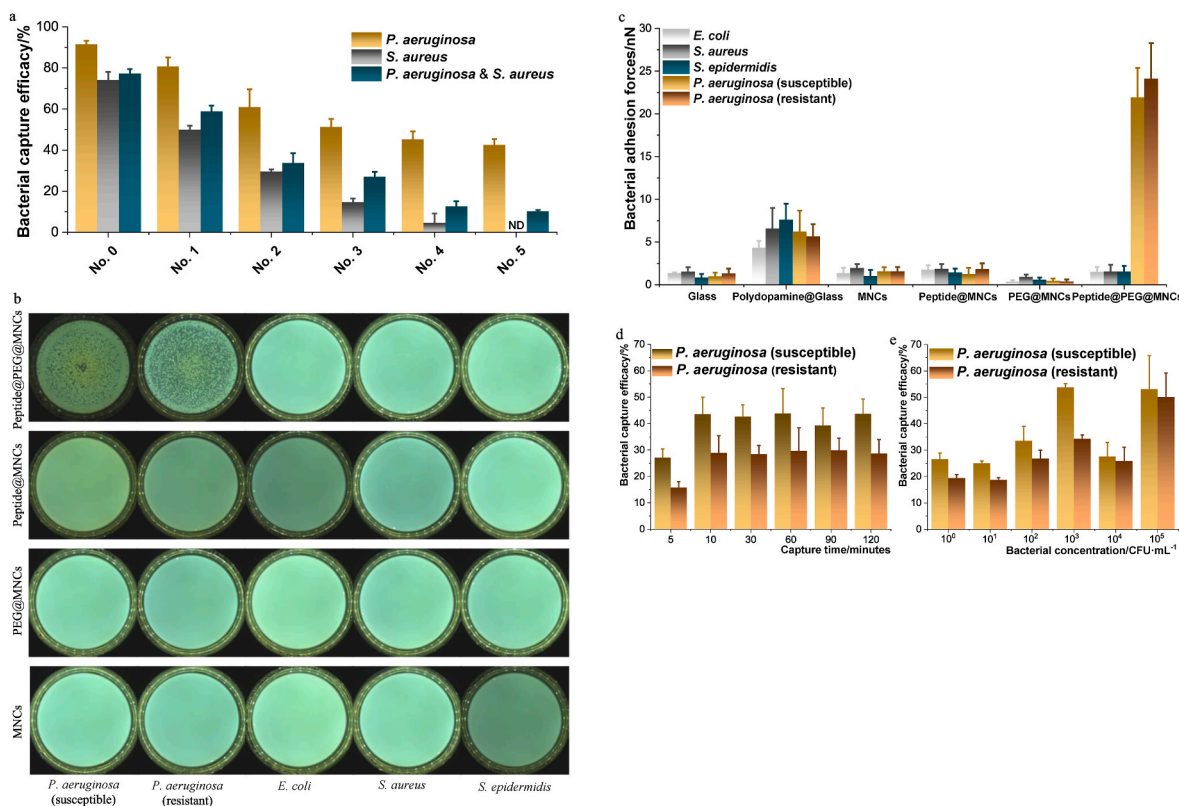
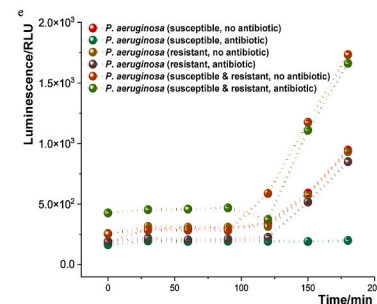
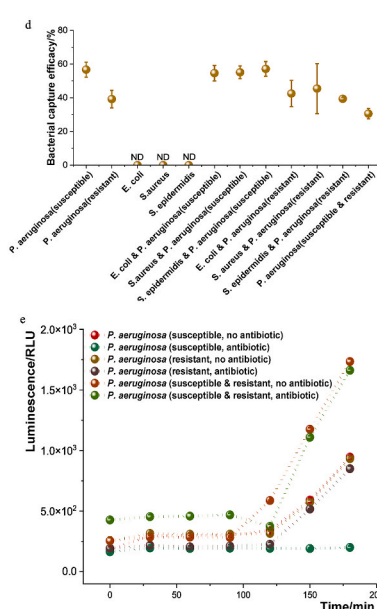
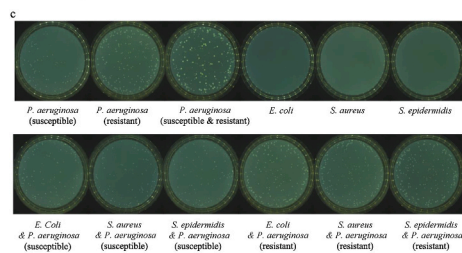
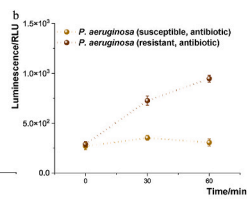
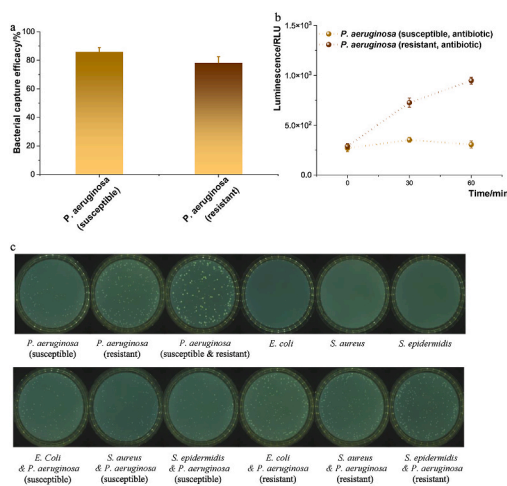


Fig. 2. Specific bacterial capture in PBS toward *P. aeruginosa* with a rinsing procedure. (a) Bacteria captured by the modified MNCs were rinsed five times to yield a specific capture of the susceptible *P. aeruginosa*. The capture efficacy from the mixed bacterial strains was aligned with the sum of initial susceptible *P. aeruginosa* and *S. aureus*. Initial concentrations of the susceptible *P. aeruginosa* and *S. aureus* were respectively 251000 ± 14000 and 803000 ± 154000 CFU mL⁻¹. (b) Specific bacterial capture through MNCs, PEG@MNCs, peptide@MNCs, and peptide@PEG@MNCs toward the susceptible and resistant *P. aeruginosa*, *E. coli*, *S. aureus*, and *S. epidermidis*. Bacteria were incubated with the nanoclusters for 10 min, and collected through a magnetic field, washed five times with PBS. The washed nanoclusters were spread on agar plates, followed by the overnight culture at 37 °C. The obtained colonies represent the collected bacteria on the nanoclusters. (c) Affinity evaluation between bacteria and modified/non-modified MNCs through single bacterial force spectroscopy. Modified/non-modified MNCs were deposited on glass petri dishes coated with polydopamine based on the published methods (Mittelviehhaus et al., 2019). (d) Evaluation of bacterial capture rate by the peptide@PEG@MNCs for the interaction of 5, 10, 30, 60, 90, and 120 min toward the susceptible and resistant *P. aeruginosa*. The concentrations of initial bacterial suspension were respectively 542000 ± 8000 and 436000 ± 38000 CFU mL⁻¹ for the susceptible and resistant *P. aeruginosa*. (e) Capture sensitivity by the peptide@PEG@MNCs toward the susceptible and resistant *P. aeruginosa* of various concentration ranges 10^5 – 10^0 CFU mL⁻¹. The concentrations of initial bacterial suspension are respectively 327000 ± 23000 and 439000 ± 39000 CFU mL⁻¹ for the susceptible and resistant *P. aeruginosa*. $n = 3$ (biological repeats), mean \pm SD shown, for (a), and (c)–(e); the analysis was at least performed independently twice, and one set of data was displayed.

(Fig. 2b). We further applied single bacterial force spectroscopy to measure the affinity between single bacterial cells and the differently functionalized magnetic nanoclusters to better understand the underlying interactions (Fig. 2c and Table S1). Similar mean adhesion forces for all evaluated strains toward the MNCs and peptide@MNCs were measured in a range of 1.0–2.0 nN. The measured affinity between the assessed pathogen *P. aeruginosa* and PEG@MNCs displayed even lower mean values in a range of 0.3–1.0 nN, probably caused by the well-known antifouling property of PEG (Lowe et al., 2015). However, the quantified affinity of the examined pathogen toward the peptide@PEG@MNCs displayed different profiles, low affinity in a range of 1.50–1.55 nN for *E. coli*, *S. aureus*, *S. epidermidis*, and high affinity toward susceptible and resistant *P. aeruginosa*, respectively, at 21.93 nN and 24.11 nN. The high affinity of *P. aeruginosa* toward the peptide@PEG@MNCs clearly demonstrated that the comparatively strong binding led to the exclusive capture of *P. aeruginosa* by the peptide@PEG@MNCs (Fig. 2b). Nevertheless, the specific capture efficiency toward the susceptible and resistant *P. aeruginosa* was sacrificed, from above 88% (Fig. 1d) to $43.7 \pm 5.6\%$ and $28.6 \pm 5.3\%$ (Fig. 2d). Hence, the developed peptide@PEG@MNCs enabled a specific capture of *P. aeruginosa* through a strong binding to the bacteria.

In order to obtain an optimized interaction time, the peptide@PEG@MNCs were incubated with *P. aeruginosa* for 5, 10, 30, 60, 90, and 120 min (Fig. 2d). It was found that 10 min interaction is sufficient to reach the maximal capture, and the prolonged incubation to 120 min did not lead to essentially better capture efficiency.

The sensitivity of the peptide@PEG@MNCs toward a specific capture through the rinsing procedure was further conducted, using various *P. aeruginosa* concentrations (10^0 – 10^5 CFU mL⁻¹ (Finer and Landau, 2004)) (Fig. 2e). We observed that both susceptible and resistant *P. aeruginosa* could be captured by exploiting the peptide@PEG@MNCs, even at an extremely low concentration (10^0 CFU·mL⁻¹, Fig. 2e), revealing that the developed peptide@PEG@MNCs were capable of a specific capture of *P. aeruginosa* with high sensitivity, which is probably originated from the higher affinity between the peptide@PEG@MNCs and the assessed *P. aeruginosa* pathogens (Fig. 2c&e and Table S1).



specifically captured bacteria was analyzed with and without $10 \mu\text{g mL}^{-1}$ gentamicin by the AquaSpark luminescence assay. $n = 3$ (biological repeats), mean \pm SD shown.

3.3. Specific capture of *P. aeruginosa* in artificial urine and rapid AMR detection

In order to simulate the condition of UTIs, artificial urine spiked with *P. aeruginosa* was exploited to further evaluate the peptide@PEG@MNCs toward bacterial capture. The capture efficiency was as high as 85.9% and 78.1%, respectively, for the susceptible and resistant *P. aeruginosa* without the rinsing procedure (Fig. 3a). The captured *P. aeruginosa* pathogens were then analyzed for antimicrobial resistance to monitor bacterial growth in the presence of antibiotics through the utilization of the AquaSpark luminescent probe (Fig. 3b) and optical density (Fig. S2a&b). The luminescent-based method allowed clear differentiation of the growth behavior for the susceptible and resistant *P. aeruginosa* after 30 min in the presence of antibiotic gentamicin, which cannot be observed through the conventional OD measurement. Moreover, the specificity of the peptide@PEG@MNCs toward *P. aeruginosa* with a rinsing process was evaluated by employing artificial urine spiked with *P. aeruginosa* and one of *E. coli*, *S. aureus*, and *S. epidermidis*. Bacterial isolation was only found for *P. aeruginosa* (Fig. 3c&d). The capture efficiencies of around 55% and 40% were obtained for the samples containing susceptible and resistant *P. aeruginosa*, respectively, regardless of the presence or absence of other bacterial strains. Thus, we could speculate that the captured bacteria were mainly *P. aeruginosa* from a suspension containing *P. aeruginosa* mixed with *E. coli*, *S. aureus*, or *S. epidermidis*. This speculation was further supported by polymerase chain reaction (PCR) analysis (Fig. S3). Hence, the developed peptide@PEG@MNCs demonstrated specificity to *P. aeruginosa*, which led to a specific capture of *P. aeruginosa* from an infected system containing single or mixed bacterial pathogens.

The isolated *P. aeruginosa* was then incubated together with gentamicin, and the relative bacterial growth was investigated by luminescence assay (Fig. 3e) and optical density (Figs. S2c–f). The observed discrepancy of the luminescent intensity appeared after incubation of 360 min for the resistant and susceptible *P. aeruginosa* (Fig. 3e), whereas no clear difference in optical density for both strains could be observed during this time frame (Figs. S2c–f), demonstrating the high sensitivity of the luminescent method.

Fig. 3. Bacterial capture in bacteria-spiked artificial urine. (a) Capture efficacies of the peptide@PEG@MNCs without rinsing process toward the susceptible and resistant *P. aeruginosa* normalized to the respective initial suspension of 715000 ± 42000 and 175000 ± 11000 CFU mL⁻¹. (b) Growth of the captured *P. aeruginosa* was assessed with and without $10 \mu\text{g mL}^{-1}$ Gentamicin through the AquaSpark luminescence assay. (c) Specific bacterial capture by the peptide@PEG@MNCs from the artificial urine spiked with susceptible-, resistant- *P. aeruginosa*, *E. coli*, *S. aureus*, *S. epidermidis*, or *P. aeruginosa* mixed with one strain *E. coli*, *S. aureus*, or *S. epidermidis*, respectively. (d) Capture toward every single bacterial strain was normalized to the corresponding initial bacterial concentration, namely susceptible *P. aeruginosa* 760000 ± 79000 CFU mL⁻¹, resistant *P. aeruginosa* 1097000 ± 35000 CFU mL⁻¹, *E. coli* 2320000 ± 157000 CFU mL⁻¹, *S. aureus* 1453000 ± 488000 CFU mL⁻¹, and *S. epidermidis* 185000 ± 23000 CFU mL⁻¹. Capture toward bacterial mixtures was respectively aligned to the susceptible and resistant *P. aeruginosa* in the presence of susceptible and resistant *P. aeruginosa*. For the mixture of susceptible and resistant *P. aeruginosa*, the sum of the initial bacterial concentration of the susceptible and resistant *P. aeruginosa* was used for alignment. N.D. represents not detected. (e) The growth of the

4. Conclusion

In this work, we successfully fabricated the PEGylated MNCs functionalized by QRKLAAKLT peptide (peptide@PEG@MNCs), yielding a removal of various bacterial pathogens and specifically capture of *P. aeruginosa* even in a low bacterial concentration. The capture specificity of *P. aeruginosa* strains by the peptide@PEG@MNCs was caused by their strong affinity confirmed with AFM analysis. Without a rinsing procedure, the capture efficacy of *P. aeruginosa* from the spiked artificial urine can be up to 85.9% and 78.1%, respectively, for susceptible and resistant *P. aeruginosa*, while with a rinsing procedure, the specific capture efficiency of *P. aeruginosa* sunk to 56.7% and 39.2%. The captured *P. aeruginosa* can be subsequently analyzed by a luminescence-based assay to monitor bacterial growth in the presence of antibiotics, which allowed rapid differentiation of the resistant and susceptible *P. aeruginosa*. The peptide@PEG@MNCs demonstrated a diagnostic potential in rapidly detecting resistant *P. aeruginosa* from UTIs for optimized treatment and minimizing the suffering of the patients. This developed method poses a theranostic prospect to combat UTIs in clinics.

CRedit authorship contribution statement

Fei Pan: Conceptualization, Methodology, Software, Validation, Formal analysis, Investigation, Visualization, Supervision, Project administration, Writing – original draft, Writing – review & editing. **Stefanie Altenried:** Methodology, Validation, Investigation. **Subas Scheibler:** Methodology, Investigation, Validation. **Alexandre H.C. Anthi:** Methodology, Investigation, Validation. **Qun Ren:** Conceptualization, Methodology, Validation, Formal analysis, Investigation, Supervision, Project administration, Writing – original draft, Writing – review & editing.

Declaration of competing interest

The authors declare that they have no known competing financial interests or personal relationships that could have appeared to influence the work reported in this paper.

Data availability

Data will be made available on request.

Acknowledgments

The authors gratefully acknowledge Irene Rodriguez Fernandez for her technical support. The authors thank Dr. Mario Hupfeld, Dr. Lukas Tanner from NEMIS Technologies AG (Dübendorf, Switzerland), and Dr. Julian Ihssen from Biosynth AG (Staad, Switzerland) for their kind support and donation concerning the AquaSpark® caprylate luminescent probe. O. Guillaume-Gentil and Nico Strohmeier are acknowledged for their kind support regarding FluidFM.

Appendix A. Supplementary data

Supplementary data to this article can be found online at <https://doi.org/10.1016/j.bios.2022.114962>.

References

Arnold, S.H., Jensen, J.N., Bjerrum, L., Siersma, V., Bang, C.W., Kousgaard, M.B., Holm, A., 2021. Effectiveness of a tailored intervention to reduce antibiotics for urinary tract infections in nursing home residents: a cluster, randomised controlled trial. *Lancet Infect. Dis.* 21 (11), 1549–1556.

Bohara, R.A., Pawar, S.H., 2015. Innovative developments in bacterial detection with magnetic nanoparticles. *Appl. Biochem. Biotechnol.* 176 (4), 1044–1058. <https://doi.org/10.1007/s12010-015-1628-9>.

Carnazza, S., Foti, C., Giofrè, G., Felici, F., Guglielmino, S., 2008. Specific and selective probes for *Pseudomonas aeruginosa* from phage-displayed random peptide libraries. *Biosens. Bioelectron.* 23 (7), 1137–1144.

Chan, J.F.-W., Yuen, K.-Y., 2015. A new ASPECT for complicated urinary tract infections. *Lancet* 385 (9981), 1920–1922.

Finer, G., Landau, D., 2004. Pathogenesis of urinary tract infections with normal female anatomy. *Lancet Infect. Dis.* 4 (10), 631–635.

Flores-Mireles, A.L., Walker, J.N., Caparon, M., Hultgren, S.J., 2015. Urinary tract infections: epidemiology, mechanisms of infection and treatment options. *Nat. Rev. Microbiol.* 13 (5), 269–284.

Franco, D., De Plano, L., Rizzo, M., Scibilia, S., Lentini, G., Fazio, E., Neri, F., Guglielmino, S., Mezzasalma, A., 2020. Bio-hybrid gold nanoparticles as SERS probe for rapid bacteria cell identification. *Spectrochim. Acta Mol. Biomol. Spectrosc.* 224, 117394.

Guo, F., Pan, F., Zhang, W., Liu, T., Zuber, F., Zhang, X., Yu, Y., Zhang, R., Niederberger, M., Ren, Q., 2022. Robust antibacterial activity of xanthan-gum-stabilized and patterned CeO₂-x-TiO₂ antifog films. *ACS Appl. Mater. Interfaces* 14 (39), 44158–44172. <https://doi.org/10.1021/acsmi.2c11968>.

Hegemann, D., Hanselmann, B., Zuber, F., Pan, F., Gaiser, S., Rupper, P., Maniura-Weber, K., Ruffieux, K., Ren, Q., 2022. Plasma-deposited AgO_x-doped TiO_x coatings enable rapid antibacterial activity based on ROS generation. *Plasma Process. Polym.* 19 (7), e2100246. <https://doi.org/10.1002/ppap.202100246>.

Hoban, D.J., Nicolle, L.E., Hawser, S., Bouchillon, S., Badal, R., 2011. Antimicrobial susceptibility of global inpatient urinary tract isolates of *Escherichia coli*: results from the study for monitoring antimicrobial resistance trends (SMART) program: 2009–2010. *Diagn. Microbiol. Infect. Dis.* 70 (4), 507–511.

Huang, X., Hürlimann, D., Spanke, H.T., Wu, D., Skowicki, M., Dinu, I.A., Dufresne, E.R., Palivan, C.G., 2022. Cell-derived vesicles with increased stability and on-demand functionality by equipping their membrane with a cross-linkable copolymer. *Adv. Healthcare Mater.*, 2202100. <https://doi.org/10.1002/adhm.202202100>.

Jin, G., Prabhakaran, M.P., Kai, D., Annamalai, S.K., Arunachalam, K.D., Ramakrishna, S., 2013. Tissue engineered plant extracts as nanofibrous wound dressing. *Biomaterials* 34 (3), 724–734.

Jokerst, J.V., Lobovkina, T., Zare, R.N., Gambhir, S.S., 2011. Nanoparticle PEGylation for imaging and therapy. *Nanomedicine* 6 (4), 715–728.

Kung, P.-Y., Cai, S.-L., Pan, F., Shen, T.-W., Su, Y.-H., 2018. Photonic fano resonance of multishaped Cu₂O nanoparticles on ZnO nanowires modulating efficiency of hydrogen generation in water splitting cell. *ACS Sustain. Chem. Eng.* 6 (5), 6590–6598. <https://doi.org/10.1021/acssuschemeng.8b00381>.

Kung, P.-Y., Pan, F., Su, Y.-H., 2020. Gold nanoparticles on TM:ZnO (TM: Fe, Co) as spinplasmon-assisted electro-optic reaction modulator in solar-to-hydrogen water splitting cell. *ACS Sustain. Chem. Eng.* 8 (39), 14743–14751. <https://doi.org/10.1021/acssuschemeng.0c03610>.

Kung, P.-Y., Pan, F., Su, Y.-H., 2021. Spintronic hydrogen evolution induced by surface plasmon of silver nanoparticles loaded on Fe- and Co-doped ZnO nanorods. *J. Mater. Chem.* 9 (44), 24863–24873. <https://doi.org/10.1039/D1TA04949F>.

Lai, H.Z., Wang, S.G., Wu, C.Y., Chen, Y.C., 2015. Detection of *Staphylococcus aureus* by functional gold nanoparticle-based affinity surface-assisted laser desorption/ionization mass spectrometry. *Anal. Chem.* 87 (4), 2114–2120. <https://doi.org/10.1021/ac503097v>.

Lai, Y.-S., Pan, F., Su, Y.H., 2018. Firefly-like water splitting cells based on FRET phenomena with ultrahigh performance over 12%. *ACS Appl. Mater. Interfaces* 10 (5), 5007–5013. <https://doi.org/10.1021/acsmi.7b18003>.

Lai, Y.-S., Del Rosario, M.A.J.V.G., Chen, W.-F., Yen, S.-C., Pan, F., Ren, Q., Su, Y.-H., 2019. Energy-yielding mini heat thermocells with WS₂ water-splitting dual system to recycle wasted heat. *ACS Appl. Energy Mater.* 2 (10), 7092–7103. <https://doi.org/10.1021/acsaem.9b01010>.

Lamas Ferreira, J.L., Álvarez Otero, J., González González, L., Novoa Lamazares, L., Arca Blanco, A., Bermúdez Sanjurjo, J.R., Rodríguez Conde, I., Fernández Soneira, M., de la Fuente Aguado, J., 2017. *Pseudomonas aeruginosa* urinary tract infections in hospitalized patients: mortality and prognostic factors. *PLoS One* 12 (5), e0178178. <https://doi.org/10.1371/journal.pone.0178178>.

Lattuada, M., Ren, Q., Zuber, F., Galli, M., Bohmer, N., Matter, M.T., Wichser, A., Bertazzo, S., Pier, G.B., Herrmann, I.K., 2016. Theranostic body fluid cleansing: rationally designed magnetic particles enable capturing and detection of bacterial pathogens. *J. Mater. Chem. B* 4 (44), 7080–7086.

Leitner, L., Ujmajuridze, A., Chanishvili, N., Goderdzishvili, M., Chkonia, I., Rigvava, S., Chkhotua, A., Changashvili, G., McCallin, S., Schneider, M.P., 2021. Intravesical bacteriophages for treating urinary tract infections in patients undergoing transurethral resection of the prostate: a randomised, placebo-controlled, double-blind clinical trial. *Lancet Infect. Dis.* 21 (3), 427–436.

Lesniewski, A., Los, M., Jonsson-Niedziolka, M., Krajewska, A., Szot, K., Los, J.M., Niedziolka-Jonsson, J., 2014. Antibody modified gold nanoparticles for fast and selective, colorimetric T7 bacteriophage detection. *Bioconjugate Chem.* 25 (4), 644–648. <https://doi.org/10.1021/bc500035y>.

Lowe, S., O'Brien-Simpson, N.M., Connal, L.A., 2015. Antibiofouling polymer interfaces: poly(ethylene glycol) and other promising candidates. *Polym. Chem.* 6 (2), 198–212. <https://doi.org/10.1039/C4PY01356E>.

Milionis, A., Tripathy, A., Donati, M., Sharma, C.S., Pan, F., Maniura-Weber, K., Ren, Q., Poulikakos, D., 2020. Water-based scalable methods for self-cleaning antibacterial ZnO-nanostructured surfaces. *Ind. Eng. Chem. Res.* 59 (32), 14323–14333. <https://doi.org/10.1021/acs.iecr.0c01998>.

Mittelviehhaus, M., Müller, D.B., Zambelli, T., Vorholt, J.A., 2019. A modular atomic force microscopy approach reveals a large range of hydrophobic adhesion forces among bacterial members of the leaf microbiota. *ISME J.* 13 (7), 1878–1882.

- Pan, F., 2022. Fighting antimicrobial resistant (AMR) bacteria: from bacteriophage-based specific capture to controlled killing. ETH Zurich.
- Pan, F., Su, Y.-H., Augusto, J., Hwang, W.-S., Chen, H.-L., 2016. Optical inclusion transformation with different amount of cerium addition during solidification of SS400 steel. *Opt. Quant. Electron.* 48 (12) <https://doi.org/10.1007/s11082-016-0795-4>.
- Pan, F., Chen, H.-L., Su, Y.-H., Su, Y.-H., Hwang, W.-S., 2017. Inclusions properties at 1673 K and room temperature with Ce addition in SS400 steel. *Sci. Rep.* 7, 2564 <https://doi.org/10.1038/s41598-017-02478-6>.
- Pan, F., Altenried, S., Liu, M., Hegemann, D., Bülbül, E., Moeller, J., Schmahl, W.W., Maniura-Weber, K., Ren, Q., 2020. A nanolayer coating on polydimethylsiloxane surfaces enables a mechanistic study of bacterial adhesion influenced by material surface physicochemistry. *Mater. Horiz.* 7 (1), 93–103.
- Pan, F., Altenried, S., Zuber, F., Wagner, R.S., Su, Y.-H., Rottmar, M., Maniura-Weber, K., Ren, Q., 2021a. Photo-activated titanium surface confers time dependent bactericidal activity towards Gram positive and negative bacteria. *Colloids Surf. B Biointerfaces* 206, 111940.
- Pan, F., Amarjargal, A., Altenried, S., Liu, M., Zuber, F., Zeng, Z., Rossi, R.M., Maniura-Weber, K., Ren, Q., 2021b. Bioresponsive hybrid nanofibers enable controlled drug delivery through glass transition switching at physiological temperature. *ACS Appl. Bio Mater.* 4 (5), 4271–4279.
- Pan, F., Altenried, S., Scheibler, S., Rodriguez Fernandez, I., Giovannini, G., Ren, Q., 2022a. Ultrafast determination of antimicrobial resistant *Staphylococcus aureus* specifically captured by functionalized magnetic nanoclusters. *ACS Sens.* 7 (11), 3491–3500. <https://doi.org/10.1021/acssensors.2c01837>.
- Pan, F., Wu, C.-C., Chen, Y.-L., Kung, P.-Y., Su, Y.-H., 2022b. Machine learning ensures rapid and precise selection of gold sea-urchin-like nanoparticles for desired light-to-plasmon resonance. *Nanoscale* 14 (37), 13532–13541.
- Pan, F., Giovannini, G., Zhang, S., Altenried, S., Zuber, F., Chen, Q., Boesel, L.F., Ren, Q., 2022c. pH-responsive silica nanoparticles for triggered treatment of skin wound infections. *Acta Biomater.* 145, 172–184.
- Pan, F., Zhang, S., Altenried, S., Zuber, F., Chen, Q., Ren, Q., 2022d. Advanced antifouling and antibacterial hydrogels enabled by the controlled thermo-responses of a biocompatible polymer composite. *Biomater. Sci.* 10 (21), 6146–6159.
- Pan, F., Liu, M., Altenried, S., Lei, M., Yang, J., Straub, H., Schmahl, W.W., Maniura-Weber, K., Guillaume-Gentil, O., Ren, Q., 2022e. Uncoupling bacterial attachment on and detachment from polydimethylsiloxane surfaces through empirical and simulation studies. *J. Colloid Interface Sci.* 622, 419–430. <https://doi.org/10.1016/j.jcis.2022.04.084>.
- Ricchizzi, E., Latour, K., Kärki, T., Buttazzi, R., Jans, B., Moro, M.L., Nakitanda, O.A., Plachouras, D., Monnet, D.L., Suetens, C., 2018. Antimicrobial use in European long-term care facilities: results from the third point prevalence survey of healthcare-associated infections and antimicrobial use, 2016 to 2017. *Euro Surveill.* 23 (46), 1800394.
- Roberts, S.C., Zembower, T.R., 2021. Global increases in antibiotic consumption: a concerning trend for WHO targets. *Lancet Infect. Dis.* 21 (1), 10–11.
- Sarigul, N., Korkmaz, F., Kurultak, I., 2019. A new artificial urine protocol to better imitate human urine. *Sci. Rep.* 9, 20159.
- Solar, P., González, G., Vilos, C., Herrera, N., Juica, N., Moreno, M., Simon, F., Velásquez, L., 2015. Multifunctional polymeric nanoparticles doubly loaded with SPION and ceftiofur retain their physical and biological properties. *J. Nanobiotechnol.* 13 (1), 14. <https://doi.org/10.1186/s12951-015-0077-5>.
- To, K.K., Lo, W.-U., Chan, J.F., Tse, H., Cheng, V.C., Ho, P.-L., 2013. Clinical outcome of extended-spectrum beta-lactamase-producing *Escherichia coli* bacteremia in an area with high endemicity. *Int. J. Infect. Dis.* 17 (2), e120–e124.
- Tong, W.-F., Liu, X.-L., Pan, F., Wu, Z.-Q., Jiang, W.-W., 2013. Protein adsorption and cell adhesion on RGD-functionalized silicon substrate surfaces. *Chin. J. Polym. Sci.* 31 (3), 495–502. <https://doi.org/10.1007/s10118-013-1210-2>.
- Tseng, M.-Y., Su, Y.-H., Lai, Y.-S., Pan, F., Kung, P.-Y., 2020. Cobalt–Citrate Metal–Organic-framework UTSA-16 on TiO₂ nanoparticles. *IOP Conf. Ser. Mater. Sci. Eng.* 720, 012008 <https://doi.org/10.1088/1757-899x/720/1/012008>.
- Wagenlehner, F., Pilatz, A., Naber, K., Weidner, W., 2008. Therapeutic challenges of urosepsis. *Eur. J. Clin. Invest.* 38, 45–49.
- Wei, J., Wang, R., Pan, F., Fu, Z., 2022a. Polyvinyl alcohol/graphene oxide conductive hydrogels via the synergy of freezing and salting out for strain sensors. *Sensors* 22 (8), 3015.
- Wei, J., Zhu, C., Zeng, Z., Pan, F., Wan, F., Lei, L., Nyström, G., Fu, Z., 2022b. Bioinspired cellulose-integrated MXene-based hydrogels for multifunctional sensing and electromagnetic interference shielding. *Interdisciplinary Mater.* 1 (4), 495–506.
- Wu, C.-C., Pan, F., Su, Y.-H., 2021. Surface plasmon resonance of gold nano-sea-urchins controlled by machine-learning-based regulation in seed-mediated growth. *Adv. Photonic. Res.* 2 (9), 2100052.
- Wu, N., Yang, Y., Wang, C., Wu, Q., Pan, F., Zhang, R., Liu, J., Zeng, Z., 2022a. Ultrathin cellulose nanofiber assisted ambient-pressure-dried, ultralight, mechanically robust, multifunctional MXene aerogels. *Adv. Mater.* 2207969 <https://doi.org/10.1002/adma.202207969>.
- Wu, N., Li, B., Pan, F., Zhang, R., Liu, J., Zeng, Z., 2022b. Ultrafine cellulose nanocrystal-reinforced MXene biomimetic composites for multifunctional electromagnetic interference shielding. *Sci. Chin. Mater.* <https://doi.org/10.1007/s40843-022-2279-3>.
- Yang, Y., Wu, N., Li, B., Liu, W., Pan, F., Zeng, Z., Liu, J., 2022. Biomimetic porous MXene sediment-based hydrogel for high-performance and multifunctional electromagnetic interference shielding. *ACS Nano* 16 (9), 15042–15052. <https://doi.org/10.1021/acsnano.2c06164>.
- Yu, R., Pan, F., Schreine, C., Wang, X., Bell, D.M., Qiu, G., Wang, J., 2021. Quantitative determination of airborne redox-active compounds based on heating-induced reduction of gold nanoparticles. *Anal. Chem.* 93 (44), 14859–14868. <https://doi.org/10.1021/acs.analchem.1c03823>.